Synthesis and properties of CSxFy thin films deposited by reactive magnetron sputtering in an Ar/SF6 discharge

Chung-Chuan Lai, Cecilia Goyenola, Esteban Broitman, Lars-Åke Näslund, Hans Högberg, Lars Hultman, Gueorgui Kostov Gueorguiev and Johanna Rosén

Journal Article

Original Publication:

Chung-Chuan Lai, Cecilia Goyenola, Esteban Broitman, Lars-Åke Näslund, Hans Högberg, Lars Hultman, Gueorgui Kostov Gueorguiev and Johanna Rosén, Synthesis and properties of CSxFy thin films deposited by reactive magnetron sputtering in an Ar/SF6 discharge, Journal of Physics, 2017. 29(19)
http://dx.doi.org/10.1088/1361-648X/aa67d2

Synthesis and properties of CS_xF_y thin films deposited by reactive magnetron sputtering in an Ar/SF_6 discharge

Chung-Chuan Lai*, Cecilia Goyenola, Esteban Broitman, Lars-Åke Näslund, Hans Högberg, Lars Hultman, Gueorgui K. Gueorguiev, Johanna Rosen

Thin Film Physics Division, Department of Physics, Chemistry and Biology (IFM), Linköping University, SE-58183 Linköping, Sweden

* Corresponding author: Chung-Chuan Lai (chula@ifm.liu.se)

Abstract

A theoretical and experimental study on the growth and properties of a ternary carbon-based material, CS_xF_y, synthesized from SF_6 and C as primary precursors is reported. The synthetic growth concept was applied to model the possible species resulting from the fragmentation of SF_6 molecules and the recombination of S-F fragments with atomic C. The possible species were further evaluated for their contribution to the film growth. Corresponding solid CS_xF_y thin films were deposited by reactive direct current magnetron sputtering from a C target in mixed Ar/SF_6 discharge with different SF_6 partial pressures (P_{SF6}). Properties of the films were determined by X-ray photoelectron spectroscopy, X-ray reflectivity, and nanoindentation. A reduced mass density in the CS_xF_y films is predicted due to incorporation of precursor species with a more pronounced steric effect, which also agrees with the low density values observed for the films. Increased P_{SF6} leads to decreasing deposition rate and increasing density, as explained by enhanced fluorination and etching on the deposited surface by a larger concentration of F/F_2 species during the growth, as supported by an increment of the F relative content in the films. Mechanical properties indicating superelasticity were obtained from the film with lowest F content, implying a fullerene-like structure in CS_xF_y compounds.

1. Introduction

Carbon-based thin films with concentration of *p*-elements below 30 at.% have become increasingly attractive due to their unique mechanical and tribological properties [1] [2] [3] [4] [5] [6] [7] as well as their good biocompatibility [8] [9]. A well-known example is the discovery of C-N thin films with fullerene-like (FL) nanostructure deposited by reactive direct current magnetron sputtering (rDCMS) [10]. The CN_x thin films exhibit high hardness, high resilience and low wear rate [11]. These properties are explained by buckling and cross-linking of the curved graphitic C-N planes in the FL structure, mixing sp^2 and sp^3 bonded carbon atoms [10] [12]. Following the discovery of CN_x thin films, the class of FL and nanostructured C-based thin solid films grew as a result of exploration of different binary systems, such as C-P, C-F, and C-S which also provide a wide range of possibilities for tuning the mechanical, electrical, optical, and chemical properties.

Studying the growth and the properties of ternary carbon-based materials, such as CS_xF_y, is also motivated by combining the effects of both hetero-elements, e.g., the increased electron mobility and the enhanced chemical inertness of S- and F-doped carbon, respectively. The differences in the atomic radius and in the electronic structure between the heteroatoms also affect the microstructure and, thus, the mechanical properties of the material. The ternary systems, therefore, provide an extra parameter to tune the properties of the carbon-based thin films compared to the binary systems.

The experimental attempts for synthesizing the CP_x, CF_x, and CS_x carbon-based thin films has been preceded by mapping out the relationship between their chemical composition and their nanostructure via computer simulations applying the synthetic growth concept (SGC). The SGC is an approach for simulation of thin film formation during vapor phase deposition based on density functional theory (DFT) [12] [13] [14] in a recursive application of candidate precursors. It has been shown that the FL structure can be obtained in all of the above mentioned systems,

but within different ranges of heteroatom concentration (up to: 30 at.% N [12], 15 at.% P [13], 15-18 at.% S [15], or 8-12 at. % F [16] [17]). This variation between the compounds is mainly explained by differences in the number of valence electrons, the electronegativity, and the steric repulsion when introducing heteroatoms belonging to different chemical elements into C-basal planes as in graphite or graphene. For example, P and S belong to the third period of the periodic table thus possessing larger covalent radii in comparison to C and N (which belong to the second period), leading to larger energy costs when the heteroatoms substitute a carbon atom in the hexagonal network [18] [19]. Fluorine, on the other hand, does not bond to more than one C atom and therefore tends to introduce severe disruptions into the network [16]. Moreover, its three other non-bonding valence electron pairs cause strong repulsion on other atoms, making the network to distort in out-of-plane directions. Thus, higher concentration of F atoms in the system introduces higher density of large-scale defects (e.g., larger rings in the network) and consequently results in different nanostructures compared to graphene-like or FL kinds of nanostructure, such as polymer-like CF_x [17].

While the theoretical understanding of the structure evolution with respect to the chemical composition was achieved for some compounds, a wide range of structural and mechanical relations of carbon-based thin films remain to be investigated. The diversity of possible process techniques/conditions also complicate the prediction and explanation of the nanostructure evolution. This implies that cases of carbon-based nanostructured films within certain range of chemical compositions should be considered in the context of the deposition process parameters. For example, the ratio between sp^2 and sp^3 bonded carbon atoms in thin films has been shown to be a function of the energetic ion bombardment and the growth temperature [20] [21] [22] [23] [24].

It is also noteworthy that the source of the heteroatom species can influence the formation of the structure in deposited thin films. As corroborated by SGC simulations, Furlan *et al*.

observed intercalation of phosphorous between graphite-like sheets in CP_x (x = 0.1 and 0.24) thin films deposited by DCMS [25] [26], as P_n clusters (n is normally 2 or 4) can be incorporated through evaporation from the surface of the compound target instead of pure sputtering deposition [27]. Furthermore, Schmidt *et al*. reported that the mechanical properties can be different for CF_x ($0.15 \leq x \leq 0.26$) thin films deposited by reactive high power impulse magnetron sputtering (HiPIMS) in Ar/CF_4 and Ar/C_4F_8 discharges, respectively [28]. An extensive SGC-based theoretical investigation was carried out for the same compounds indicating that different dissociation behaviors of the reactive gas species lead to different bonding conditions for C-atoms, thus defining different structure and properties.

Previously, the ternary FL structure was predicted by SGC simulations as feasible to be obtained in the C-S-F system for ([S] + [F]) < 10 at.%. Meanwhile, indications of graphitic structure were observed in the CS_xF_y thin films with the mentioned range of heteroatom concentrations deposited by rDCMS with a mixed Ar/SF_6 discharge [29]. Nevertheless, it remains to be determined how SF_6, as the primary precursor, affects the growth of CS_xF_y thin films, and resulting physical and mechanical properties. Also, even though the SF_6 gas is a common dry etchant for Si-based (e.g., Si [30] and SiC [31]) or metallic (e.g., W [32]) materials in plasma processes, this gas is less reported as a single source for both F and S species in reactive deposition. Thus, studies dedicated to the precursor's dissociation and reaction behaviors, as well as the relationship between the obtained properties in the CS_xF_y films and the process parameters, are needed in order to understand the formation of the C-S-F networks in the reactive deposition process.

Here, theoretical calculations were carried out for studying the dissociation of SF_6 gas into S-F fragments and the following formation of different C-S-F precursor species in a C target magnetron sputtering process. Also, CS_xF_y thin films were deposited at three different SF_6 partial pressures, P_{SF6} = 1.0 mPa, 1.5 mPa and 2.0 mPa. Their chemical composition was

quantified by X-ray photoelectron spectroscopy (XPS). The deposition rate and density of the samples were acquired from X-ray reflectivity (XRR) patterns while their mechanical properties were studied by nanoindentation. The effects of SF_6, in terms of its partial pressure during depositions, on the microstructure of the CS_xF_y samples were qualitatively elaborated based on the theoretical precursor studies and the measured properties.

2. Computational Details

The SGC [12] [13] [33] was used to model the precursor species most relevant to film formation during vapor phase deposition. The $C_pS_qF_r$ (p, $q \leq 2$, $r \leq 6$) species were studied by geometry optimization and calculation of the corresponding cohesive energy. The cohesive energy per atom (E_{coh}/at.) is defined as the energy needed to break the system into isolated atoms normalized by the total number of atoms, and is calculated according to:

$$E_{\text{coh}} = -\frac{E_{\text{total}} - \sum_j N_j \cdot E_j}{\sum_j N_j}$$

, where E_{total} is the total energy of the relaxed species, E_j and N_j correspond to the energy of the isolated atoms and the total number of atoms for different species j = {C, S, and F}.

The framework adopted for the calculations is density functional theory (DFT) within the generalized gradient approximation (GGA) as implemented in Gaussian 09 [34]. The results reported here were obtained using the Perdew-Wang exchange and correlation functional (PW91) [35] with the 6-31G** basis set. These choices have been shown to provide an accurate description for similar systems [36] [37].

3. Experimental Details

3.1 Reactive sputtering of thin films

CS_xF_y thin films were synthesized onto Si(001) substrate by rDCMS in a high vacuum system with a base pressure below 0.1 mPa, as the system previously described in Ref. [25] and [26]. All depositions were carried out with a 2-inch C target (99.9% purity, pyrolytic graphite with density ~1.8 g/cm^3) attached to a type II unbalanced magnetron operated at a constant power of 90 W, a deposition time of 120 min, and floating potential to the substrates. The magnetron was placed at a distance of 12 cm right below a substrate holder. The Si substrates were cleaned sequentially in acetone, ethanol, and isopropanol ultrasonic baths for 10 min. each, then blown dry with N_2 gas. Prior to depositions, the base pressure of the system was throttled up to 0.5 mPa and the reactive gaseous precursor SF_6 (99.993 % purity, Solvay Fluor GmbH) was supplied from a pressurized gas bottle through a leak valve up to the desired P_{SF6}, followed by additional Ar gas filled up to a working pressure of 533 mPa (4 mTorr). The CS_xF_y samples were deposited at 350 °C and at three different SF_6 partial pressures: one sample at P_{SF6} = 1.0 mPa and 1.5 mPa, and two samples at P_{SF6} = 2.0 mPa.

3.2 Sample characterization

3.2.1 X-ray photoelectron spectroscopy (XPS)

The XPS were performed with the AXIS Ultra^{DLD} system from Kratos Analytical Ltd. using monochromatic Al K_α radiation. Relative chemical composition of C, S, F, and O in the thin films was obtained by elemental quantitative analysis based on the peak areas acquired from XPS high resolution scans of the C1s, S2p, F1s, and O1s regions together with the elemental sensitivity factors, provided by *Kratos Analytical Ltd*. In order to reduce surface contamination, the samples were directly transferred from the deposition system and into the XPS system with an atmosphere exposure of only about 10 min. No sputter cleaning on the film surface was

performed before acquiring the XPS spectra, thus minimizes damage to the chemical bonding structure of the films.

3.2.2 X-ray reflectivity (XRR)

The XRR patterns of the films were acquired in an X-ray diffractometer (*Empyrean, PANalytical B.V.*) using CuKα radiation. The films were aligned for the height at 0° and for the tilt angle at 0.5° to improve the accuracy of the measurements. The acquired patterns were thereafter fitted by PANalytical X'Pert Reflectivity program with a single carbon layer on silicon substrate model in order to obtain the thickness and the density information of the films. This method has been used in Ref. [24] to determine the density of the CN_x thin films. The film thickness is thereafter divided by the total deposition time (120 min.) giving the deposition rate of the samples.

3.2.3 Nanoindentation

Nanomechanical properties of the films were evaluated by quasi-static displacement-controlled nanoindentation experiments in a TI950 TriboindenterTM (Hysitron). Hardness (*H*) and reduced modulus (*Er*) measured with a Berkovich diamond probe with a blunt-ended tip curvature of radius of ~100 nm were calculated according to the method proposed by Oliver and Pharr [38]. The tip function area at low penetration depths was calibrated using a fused silica sample. In order to avoid substrate effects, penetration displacement was set to 10% of the total coating thickness. In all tests a total of 12 indents with a spacing of 10 μm were averaged to determine the mean value and standard deviations of *H* and *Er*.

4. Results and Discussion

4.1 Theoretical study on precursor species

Precursor species $C_pS_qF_r$ (p, $q \leq 2$; $r \leq 6$) that are relevant to the here reported deposition process, (a graphite target and SF_6 reactive gas), were modeled in order to define their possible role during film formation of CS_xF_y. These species are expected to originate from the fragmentation of the SF_6 molecule,

$$SF_6 \rightarrow SF_r + (6 - r)F, \qquad \text{(R1)}$$

and from recombination reactions in the plasma or at the target surface,

$$P + P' \rightarrow PP', \qquad \text{(R2)}$$

where both *P* and *P'* are the precursor species C, S, F or SF_r fragments, and *PP'* is a recombined species. For this particular study only those recombination reactions involving one collision were taken into account.

For all composition of precursor species considered here, alternative geometric isomers were taken into account in order to find the most stable precursor geometries. The following groups of possible precursor species were optimized, compared, and considered in the context of film formation:

(i) species resulting from the fragmentation of the SF_6 molecule: SF_5, SF_4, SF_3, SF_2, and SF (as in reaction R1);

(ii) dimers resulting from the recombination of two single atomic species C, S, and F, i.e., C_2, S_2, F_2, CS, CF, and SF (as in reaction R2);

(iii) medium-size species originating from the recombination of a single atomic species and a SF_r fragment: C–SF_r, S–SF_r, and F–SF_r (as in reaction R2);

(iv) larger species originating from the recombination of two equal or different SF_r fragments: (SF_r)–$(SF_{r'})$ (as in reaction R2).

It is noteworthy that SF and F–SF_r from groups (ii) and (iii), respectively, are resulting in the same species listed in group (i) plus SF_6 molecule, and hence they will be denoted below as SF_r. The resulting stable structures for the most relevant precursor species are shown in Fig. 1 and Fig. 2, and their cohesive energies are listed in Table 1 and Table 2.

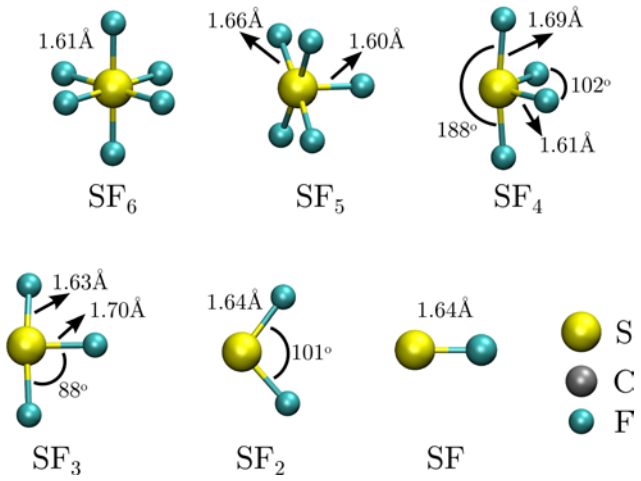

Figure 1. The most stable geometries for SF_r species resulting from the fragmentation of the SF_6 molecule.

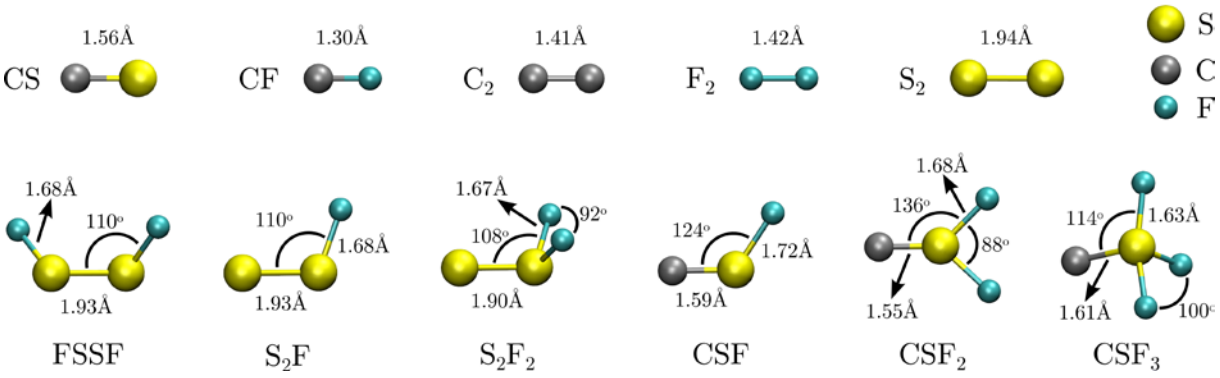

Figure 2. The most stable geometries for possible precursor species resulting from recombination reactions in the plasma, that is likely to play a significant role in the film formation process. For the FSSF precursor species, the dihedral angle (FSSF) is 89°.

Table 1. $E_{coh/at}$ for the reactive gas molecule SF_6 and the possible precursor species resulting from its fragmentation, also shown in Fig 1.

Species	SF_6	SF_5	SF_4	SF_3	SF_2	SF
$E_{coh/at}$ (eV/at)	-3.15	-2.94	-3.08	-2.80	-2.70	-2.00

Table 2. $E_{coh/at}$ for possible precursor species resulting from recombination reactions in the plasma, that is likely to play a significant role in the film formation process, also shown in Fig. 2.

Species	CS	CF	C_2	F_2	S_2	S_2F
$E_{coh/at}$ (eV/at)	-3.82	-3.21	-2.36	-1.29	-1.85	-2.66
Species	S_2F_2	FSSF	CSF	CSF_2	CSF_3	
$E_{coh/at}$ (eV/at)	-2.85	-2.83	-3.06	-2.86	-2.59	

The role of these precursor species during film formation was evaluated according to their stabilities, relative size, and accessible dangling bonds. For example, those relatively large species (e.g., SF_5) were considered to have reduced contribution to the film formation, seen from their complete electron shells and relatively high number of bonded F atoms screen the valence electrons of C and S atoms that are responsible for interacting with the dangling bonds on the growing film surface. Consequently, these larger species become geometrically less accessible to bond to the surface. From these bonding conditions, we envisage the following situations in order of increasing importance for film formation:

(1) (SF_r)–$(SF_{r'})$ fragments (r, r' = 2 – 5) should have a reduced to no impact on the film formation process;

(2) X–SF_5, X–SF_4, SF_5, and SF_4 (X = C or S) show a low number of dangling bonds in relation to their size, presenting lower likelihood of bonding onto the growing film surface;

(3) X–SF_3, X–SF_2, SF_3, and SF_2 (X = C or S) show higher chances of bonding compared to (2) but represent medium size species that will sterically prevent other precursor species from bonding in their vicinity. The prevalence of these species hints to the formation of films with low density;

(4) FS–SF, X–SF species (X = C or S), dimers and single atomic species are the most significant precursor species for growing well-structured and dense films due to their geometrical availability of dangling bonds and their smaller size.

Our evaluation shows that the precursor species with medium and smaller relative size, i.e., group (3) and (4), can contribute to most of the film growth, while the larger precursor species, i.e., group (1) and (2), have a much reduced probability to be deposited. Furthermore, properties of deposited CS_xF_y, e.g., mass density and chemical composition, can be affected by relative

amount of the above classified groups of precursor species created during the growth due to the steric effect of differently sized species on the surface.

4.2 Synthesis and characterization of CS_xF_y thin films

Solid CS_xF_y thin films were prepared by rDMCS in an Ar/SF_6 discharge using three different P_{SF6}. Fig. 3(a) summarizes the XPS quantified F and S atomic content, [F] and [S] respectively, of the CS_xF_y samples against the respective P_{SF6} used during deposition. The similar chemical composition of the samples from repeated deposition at P_{SF6} = 2.0 mPa suggests that the CS_xF_y thin film deposition by reactive sputtering with SF_6 gas is a reproducible process. The XPS spectra of C 1s, F 1s, and S 2p acquired from the samples are shown in Fig. S1 – S3 in the supplementary material. All samples have a close to constant O content in a range of 1.0 – 1.3 at.%. Notice that this [O], determined by XPS, is likely overestimated due to post-deposition oxidation on the film surface following a short exposure to air during sample transfer.

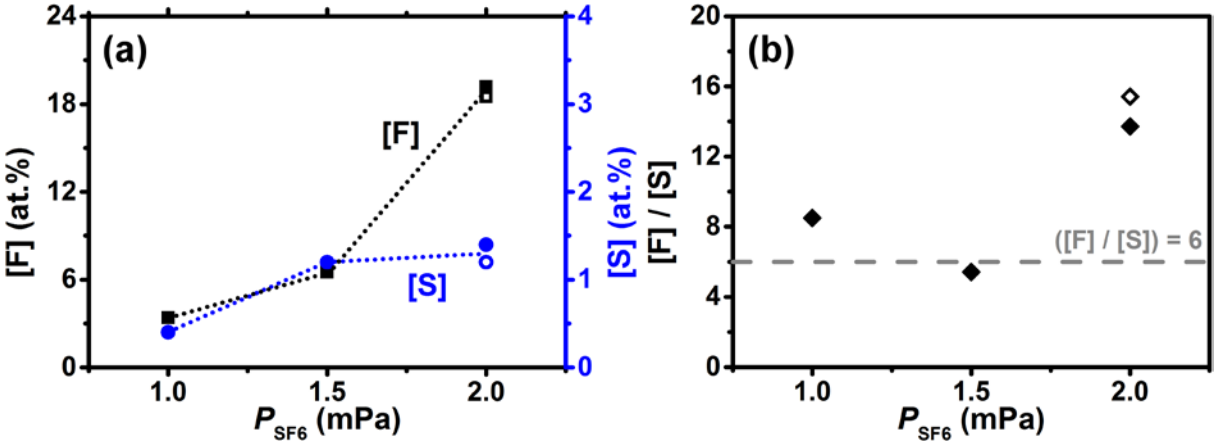

Figure 3. (a) The F and S atomic content ([F] and [S], respectively) and (b) the [F] / [S] ratio of the CS_xF_y samples plotted against P_{SF6}. The dashed line in (b) indicates the [F] / [S] ratio of a SF_6 molecule. When P_{SF6} = 2.0 mPa, solid and hollow symbols are used to distinguish the two samples.

The increment in concentration of both [F] and [S] from P_{SF6} = 1.0 mPa to 2.0 mPa suggests that the amount of the SF_6 partial pressure has a positive effect on incorporating both S and F atoms into the CS_xF_y films. Individually, a steeper increment of [F] is observed between P_{SF6} = 1.5 mPa to 2.0 mPa compared to the [F] increment between P_{SF6} = 1.0 mPa to 1.5 mPa. In contrast, the amount of [S] in the films does not show a significant change after P_{SF6} = 1.5 mPa.

The individual behaviors of F and S atoms in the reactive process are more visible by plotting the F-to-S atomic ratio of the samples against the SF_6 partial pressure, as shown in Fig. 3(b). In the figure, larger deviations from the chemical formula of the SF_6 precursor, where [F]/[S] = 6, are observed for the samples deposited at P_{SF6} = 2.0 mPa than those deposited at lower P_{SF6}. The increment in this composition ratio suggests a change in the behavior for the F- and S-containing precursor species to a regime permitting the former to remain in the films more abundantly, thus making higher and higher amount of F atoms to be incorporated during the deposition at higher P_{SF6}.

On one hand, such change of incorporation behavior can be explained by the differences in the sticking coefficient and in the dissociation behavior of the precursor species. According to the precursors' evaluation in Section 4.1, the larger size species with less geometrically accessible dangling bonds, i.e., X–SF_r and SF_r ($r \geq 4$) in group (1) and (2), should be more easily impeded to stick to the surface, while the S-containing medium and smaller size species, i.e., X–SF_r and SF_r ($r \leq 3$), FS–SF, S_2, and S in group (3) and (4), are energetically less favorable to create [39]. It has been experimentally demonstrated that the most abundant species from SF_6 discharges are the neutral or ionized molecules of F, F_2 and SF_r fragments ($r \geq 3$) [40] [41]. Hence, when depositing at higher P_{SF6}, the F_2, CF, and F species become relatively more abundant and, thus, more dominating in the growth than S-containing groups.

On the other hand, a more pronounced reactive *etching* process is expected on the deposited surface during growth at higher P_{SF6}, where the F/F_2 species, created by the fragmentation of SF_6 molecules in a plasma process, become more abundant in the deposition ambient [42] [43]. Exposing C-based materials to such environment leads to both fluorination and etching at the surface, while both reactions are enhanced as the partial pressure of SF_6 increases [44] [45]. As discussed in Section 4.1, the precursor species X–SF_r and SF_r (r = 2 or 3) from group (3) attached to the surface can locally reduce the density due to a more pronounced steric effect than group (4) species. Hence, the close-by regions are more permeable to the primary oxidants, F and F_2, and thus more susceptible to etching. As P_{SF6} increases and the etching process is promoted, more group (3) species (than only F-containing species due to generally stronger bonded F atoms) are removed from the surface and consequently the [F]/[S] ratio raises.

The significant role played by the etching effect, is supported by a decrease of the deposition rate. In Fig. 4, the total thickness of the films determined by XRR is 225 nm, 190 nm and 164 – 165 nm for the samples deposited at P_{SF6} = 1.0 mPa, 1.5 mPa, and 2.0 mPa, respectively, which is corresponding to a decreasing deposition rate from 1.88 nm/min., 1.58 nm/min., down to 1.37 – 1.38 nm/min.

In addition to the deposition rate, the shift towards higher critical angle in Fig. 4 indicates an increment in the respective mass density, *Dx*, of the samples from 1.5 to 1.9 g/cm^3 along with increasing P_{SF6} from 1.0 mPa to 2.0 mPa. The mass density of the CS_xF_y samples is considered lower than the commonly reported values for graphite (2.3 g/cm^3) [46], for tetra-amorphous carbon (1.8 – 2.2 g/cm^3) [47], and for CF_x thin films (~2.1 g/cm^3) with close chemical compositions ([F] < 26 at.%) deposited in mixed Ar/CF_4 and Ar/C_4F_8 discharges [28] [48].

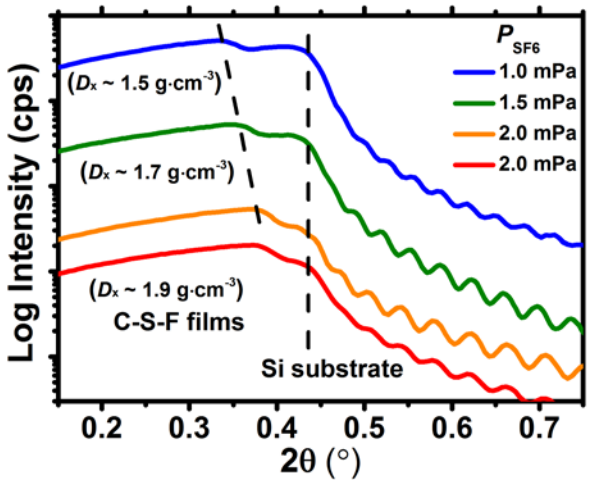

Figure 4. The XRR patterns around the critical angle of the CS_xF_y samples. The critical angles of the films and of the Si substrates are indicated with respective dashed lines.

The low mass density is similar to reported polymer-like C-based thin films, but only when the content of heteroatom species is above 25 to 30 at.% [28] [49]. Contrarily in this work, such low mass density (1.5 – 1.7 g/cm^3) of the samples deposited at low P_{SF6} is explained by the incorporation of the medium size species X–SF_r and SF_r (r = 2 or 3), i.e., group (3) species in Section 4.1, which hinder the formation of dense structure in the films. These low density regions are more efficiently removed due to the promoted selective etching at higher P_{SF6} (as explained in the previous paragraph) leading to more densified thin films (1.8 – 1.9 g/cm^3).

The nanoindentation load-displacement curves for the three samples of CS_xF_y thin films (obtained at P_{SF6} = 2.0 mPa, 1.5 mPa, and 1.0 mPa, respectively) are presented in Figure 5(a). Changes on the mechanical properties caused by introducing S and F heteroatoms into the C network can be observed by comparing the shape of the curves with curves reported previously

for pure C sample deposited at similar set-up in the same deposition system. See Fig 3(b) of Ref. [25] where the pure C sample exhibits a recovery value of ~50 %, which is significantly lower than the recovery values of the CS_xF_y samples in this work (> 75 %).

The hardness and the reduced elastic modulus of films determined by nanoindentation are summarized in Figure 5(b), where the values for the samples from repeated depositions at P_{SF6} = 2.0 mPa are, again, in good agreement with each other. Both *H* and *Er* values follow a similar trend, which increases from P_{SF6} = 1.0 mPa to 1.5 mPa and then decreases when P_{SF6} further increases to 2.0 mPa, with the minimum values observed at the lowest SF_6 partial pressure. However, the behavior of the *H* and *Er* as a function of the P_{SF6} is not monotonous as is the case with the chemical composition, the deposition rate, and the density.

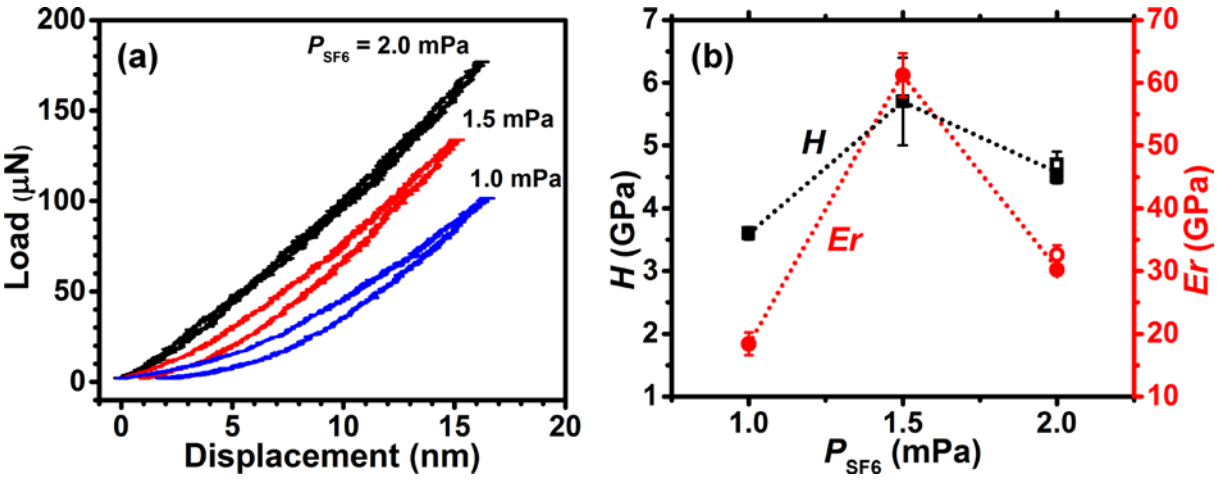

Figure 5. (a) Nanoindentation load-displacement curves of CS_xF_y thin films. (b) The hardness (*H*, squares) and the reduced elastic modulus (*Er*, circles) of CS_xF_y thin films plotted against P_{SF6}. When P_{SF6} = 2.0 mPa, solid and hollow symbols are used to distinguish between two samples, coupled to Figure 3.

The lower *H* and *Er* values of the sample deposited at P_{SF6} = 1.0 mPa, which possesses an overall heteroatom content of less than 5 at.%, are possibly due to its underdense structure. The enhancement of the mechanical properties between P_{SF6} = 1.0 – 1.5 mPa can therefore be attributed to the structural evolution of the film due to the removal of the medium size species X–SF_r and SF_r (r = 2 or 3) from the film surface by the etching effect.

As shown by theoretical modelling, the incorporation of F and/or S atoms in the network introduces local distortions, consequently enhancing the cross-linking and buckling between neighboring hexagonal (originally graphene-like) networks [15] [17] [29]. In Ref. [29], an increasing curvature of a planar carbon network is observed, when the ([F] + [S]) content is increased from 4.8 at.% to 7.1 at.%. For compounds with ([F] + [S]) ≤ 10 at.%, the incorporated defects in the graphene-like network are predicted to have positive effects on their mechanical properties. This discussion corroborates the explanation for the improvement on the mechanical properties of the samples between P_{SF6} = 1.0 – 1.5 mPa.

When an even higher amount of heteroatoms is incorporated, corresponding to the transition from P_{SF6} = 1.5 mPa to 2.0 mPa, *H* and *Er* decrease even if higher mass density values were observed. Such results are explained by the fragmentation of the highly fluorinated networks due to the termination of, mainly, F atoms. Theoretical calculations have shown that a more disrupted and strongly distorted network is observed for values of ([F] + [S]) = 9.5 at.% or higher, especially when [F] > [S] (in contrast to the cases featuring lower heteroatom content (4.8 and 7.1 at.%) [29]. Consequently, it is reasonable to expect more defective structure when [F] > 18 at.% and [F] + [S] ≈ 20 at.%, and a degradation in the hardness and elasticity of the samples grown at highest SF_6 partial pressure. Exhibiting a very similar trend, in Ref. [28], the binary CF_x thin films deposited with reactive gases of CF_4 or C_4F_8 soften when the F content increases above 15 at.%.

Despite that [F] for all samples considered in this work is significantly lower than its observed threshold for transition to polymer-like structure ([F] > 26 at.%) reported in Ref. [28], both the values for H (3 – 6 GPa) and Er (15 – 65 GPa) belong to a similar range as in the case of the binary polymer-like CF_x samples [28]. Again, this can be perceived as resulting from a less dense microstructure caused by the incorporation of the group (3) precursor species, which is also consistent with previous observation on the low mass density. In addition to the precursor's effect, an inherent lack of energetic ion bombardment in DCMS can not only cause under-dense microstructure [50], but also leads to less sp^3-hybridized bonding between C atoms [22]. Hence, in general softer films are deposited by DCMS as compared to films deposited by, for example HiPIMS, as in Ref. [28].

The hardness-to-modulus ratio (H / Er), sometimes referred as the plasticity index of a material, is calculated to be 0.20, 0.09, and 0.15 for the samples deposited at P_{SF6} = 1.0 mPa, 1.5 mPa and 2.0 mPa, respectively. A material is considered to be more elastic and compliant when its (H / Er) ratio is higher. For example, (H / Er) ratio of an elastic material, such as diamond-like carbon, is commonly found to be about 0.1, while for a super-elastic material, such as FL-CN_x, values in the range of 1.5 – 1.9 have been reported [51]. Due to the dominating fluorine content to the sulfur content of the samples in this work, it is logical to compare their properties to those in another chemically similar binary system, i.e., C-F system. It turns out that the CS_xF_y samples grown at higher P_{SF6} partial pressures ($P_{SF6} \geq 1.5$ mPa) possess (H / Er) values comparable to those of CF_x thin films with similar heteroatom content (10 – 30 at.%), e.g., of samples grown by HiPIMS (0.11 – 0.12) [28] and grown by chemical vapor deposition (~ 0.1) [52].

Additionally, a higher compliance, (H / Er) = 0.19, of the sample deposited at P_{SF6} = 1.0 mPa is obtained compared to the other samples in this work as well as the samples reported in Ref. [28] and [52]. Interestingly, this compliance value is comparable to that of the $CN_{0.13}$ thin film reported in Ref. [51], where the authors claimed superelasticity of that sample due to its FL-

structure. The similarity in their unique plasticity index may indicate the possibility for the existence of FL-structure (or at least close-order structure) in the CS_xF_y thin film deposited at P_{SF6} = 1.0 mPa. Such result is in agreement with the previous theoretical predictions on obtaining FL-structure in CS_xF_y samples with [F] + [S] < 10 at.% and the experimental observation of graphite-like feature in the CS_xF_y thin film with [F] + [S] ~ 3.8 at.% [29].

It should be noted that the mechanical properties of the sample deposited at P_{SF6} = 1.0 mPa are significantly inferior to those typically observed in FL thin films such as FL-$CN_{0.13}$ from Ref. [51]. As discussed above, such inferior mechanical properties are due to the formation of under-dense microstructure at lower SF_6 partial pressure. Our earlier transmission electron microscopy studies of the CS_xF_y sample with [F] + [S] ~ 3.8 at.% showed a corresponding lack of long-range order [29]. In other words, the fullerene-likeness, i.e., the scale of FL-structural patterns, is reduced due to the incorporation of the relatively massive S-containing species in the CS_xF_y thin film.

5. Conclusions

Growth of the ternary carbon-based CS_xF_y thin films by rDCMS using SF_6 as reactive gas was studied by characterizing the properties of the films and by evaluating the interaction of the predicted C-S-F reactant species with the structure formation of CS_xF_y. The theoretical evaluation suggested that the film growth is mainly from the interaction of medium size (X–SF_r and SF_r; X = C or S; r = 2 or 3) and smaller size (C–SF, S_2F, FS–SF, dimers, and atoms) species with more geometrically accessible dangling bonds to react with the surface. In addition, the medium sized species are likely to introduce under-dense structure to the surface due to the more pronounced steric effect, which is in a good agreement with experimentally observed low mass density values of the CS_xF_y thin films. The under-dense surface is expected to allow more effective fluorination or etching from F_2, CF, and F species, indicating by the increments in the

mass density and the decreased deposition rate when increasing P_{SF6}. Consequently, the under-dense structure and high amount of F-termination result in low values of the hardness and elastic modulus of the films deposited at low and high P_{SF6}, respectively. The mechanical compliance values indicate that most of the CS_xF_y thin films are highly elastic, and especially that the sample with the lowest heteroatom content exhibits superelastic behavior, which is a characteristic of carbon thin films with the FL structure. The changes in micro- and the nanostructure, and consequently the properties, over a small P_{SF6} change (1.0 mPa) indicate a strong dependence of the CS_xF_y thin film formation on the SF_6 partial pressure and the dissociation characteristic of SF_6.

Acknowledgments

J.R., C.G., and G.K.G. are grateful for the support by Swedish Foundation for Strategic Research (SSF) Synergy Grant #RMA11-0029 on Functional Carbides and Advanced Surface Engineering (FUNCASE). L.H, C.G., and G.K.G acknowledge the Linköping Linnaeus Initiative on Novel Functionalized Materials (VR), and FunMat (Functional Nanoscale Materials) – a VINN Excellence Centre (Swedish Agency for Innovation Systems VINNOVA). E. B., H. H., J.R., and L. H. acknowledge financial support from the Swedish Government Strategic Research Area in Materials Science on Functional Materials at Linköping University (Faculty Grant SFO Mat LiU No. 2009-00971).

References

[1] J. Robertson, Diamond-like amorphous carbon, *Mater. Sci. Eng. R* 37 (2002) 129-281.

[2] C. A. Charitidis, Nanomechanical and nanotribological properties of carbon-based thin films: A review, *Int. J. Refract. Met. H.* 28 (2010) 51-70.

[3] A. Erdemir and C. Donnet, Tribology of diamond-like carbon films: recent progress and future prospects, *J. Phys. D: Appl. Phys.* 39 (2006) R311-R327.

[4] M. P. Johansson, N. Hellgren, T. Berlind, E. Broitman, L. Hultman, and J.-E. Sundgren, Growth of CN_x/BN:C multilayer films by magnetron sputtering, *Thin Solid Films* 360 (2000) 17-23.

[5] L. Hultman, J. Neidhardt, N. Hellgren, H. Sjöström, and J.-E. Sundgren, Fullerene-like carbon nitride: a resilient coating material, *MRS Bull.* 28 (2003) 194-202.

[6] A. Zocco, A. Perrone, E. Broitman, Zs. Czigany, L. Hultman, M. Anderle, and N. Laidani, Mechanical and tribological properties of CN_x films deposited by reactive pulsed laser ablation, *Diam. Relat. Mater.* 11 (2002) 98-104.

[7] E. Broitman, J. Neidhardt, and L. Hultman, Fullerene-like Carbon Nitride: A New Carbon-based Tribological Coating in: Tribology of Diamond-like Carbon Films: Fundamentals and Applications, C. Donnet and A. Erdemir, Eds., Springer, New York, 2007, pp. 620-653.

[8] C. A. Love, R. B. Cook, T. J. Harvey, P. A. Dearnley, and R. J. K. Wood, Diamond like carbon coatings for potential application in biological implants-a review, *Tribol. Int.* 63 (2013) 141-150.

[9] E. Broitman, W. Macdonald, N. Hellgren, G. Radnóczi, Zs. Czigany, A. Wennerberg, M. Jacobsson, and L. Hultman, Carbon nitride films on orthopedic substrates, *Diam. Relat. Mater.* 9 (2000) 1984-1991.

[10] H. Sjöström, S. Stafström, M. Boman, and J.-E. Sundgren, Superhard and elastic carbon nitride thin films having fullerenelike microstructure, *Phys. Rev. Lett.* 75 (1995) 1336-1339.

[11] E. Broitman, N. Hellgren, O. Wänstrand, M. P. Johansson, T. Berlind, H. Sjöström, J.-E. Sundgren, M. Larsson, and L. Hultman, Mechanical and tribological properties of CN_x films deposited by reactive magnetron sputtering, *Wear* 248 (2001) 55-64.

[12] G. K. Gueorguiev, J. Neidhardt, S. Stafström, and L. Hultman, First-principles calculations on the curvature evolution and cross-linkage in carbon nitride, *Chem. Phys. Lett.* 410 (2005) 228-234.

[13] G. K. Gueorguiev, A. Furlan, H. Högberg, S. Stafström, and L. Hultman, First-principles calculations on the structural evolution of solid fullerene-like CP_x, *Chem. Phys. Lett.* 426 (2006) 374-379.

[14] G. K. Gueorguiev, E. Broitman, A. Furlan, S. Stafström, and L. Hultman, Dangling bond energetics in carbon nitride and phosphorus carbide thin films with fullerene-like and amorphous structure, *Chem. Phys. Lett.* 482 (2009) 110-113.

[15] C. Goyenola, S. Stafström, L. Hultman, and G. K. Gueorguiev, Structural patterns arising during synthetic growth of fullerene-like sulfocarbide, *J. Phys. Chem. C* 116 (2012) 21124-21131.

[16] G. K. Gueorguiev, C. Goyenola, S. Schmidt, and L. Hultman, CF_x: A first-principles study of structural patterns arising during synthetic growth, *Chem. Phys. Lett.* 516 (2011) 62-67.

[17] C. Goyenola, S. Stafström, S. Schmidt, L. Hultman, and G. K. Gueorguiev, Carbon fluoride, CF_x: structural diversity as predicted by first principles, *J. Phys. Chem. C* 118 (2014) 6514-6521.

[18] A. Furlan, G. K. Gueoguiev, H. Högberg, S. Stafström, and L. Hultman, Fullerene-like CP_x: A first-principles study of the relative stability of precursors and defect energetics during synthetic growth, *Thin Solid Films* 515 (2006) 1028-1032.

[19] C. Goyenola, G. K. Gueoguiev, S. Stafström, and L. Hultman, Fullerene-like CS_x: A first-principles study of synthetic growth, *Chem. Phys. Lett.* 506 (2011) 86-91.

[20] P. J. Fallon, V. S. Veerasamy, C. A. Davis, J. Robertson, G. A. J. Amaratunga, W. I. Milne, and J. Koskinen, Properties of filtered-ion-beam-deposited diamondlike carbon as a function of ion energy, *Phys. Rev. B* 48 (1993) 4777-4782.

[21] M. C. Polo, J. L. Andújar, A. Hart, J. Robertson, and W. I. Milne, Preparation of tetrahedral amorphous carbon films by filtered cathodic vacuum arc deposition, *Diam. Relat. Mater.* 9 (2000) 663-667.

[22] N. Hellgren, M. P. Johansson, E. Broitman, L. Hultman, and J.-E. Sundgren, Role of nitrogen in the formation of hard and elastic CN_x thin films by reactive magnetron sputtering, *Phys. Rev. B* 59 (1999) 5162-5169.

[23] J. Neidhardt, L. Hultman, E. Broitman, T. W. Scharf, and I. L. Singer, Structural, mechanical and tribological behavior of fullerene-like and amorphous carbon nitride coatings, *Diam. Relat. Mater.* 13 (2004) 1882-1888.

[24] M. D. Tucker, Zs. Czigány, E. Broitman, L.-Å. Näslund, L. Hultman, and J. Rosen, Filtered pulsed cathodic arc deposition of fullerene-like carbon and carbon nitride films, *J. Appl. Phys.* 115 (2014) 144312.

[25] A. Furlan, G. K. Gueorguiev, Zs. Czigány, H. Högberg, S. Braun, S. Stafström, and L. Hultman, Synthesis of phosphorus-carbide thin films by magnetron sputtering, *Phys. Stat. Sol. RRL* 2 (2008) 191-193.

[26] A. Furlan, G. K. Gueorguiev, Zs. Czigány, V. Darakchieva, S. Braun, M. R. Correia, L. Hultman, and H. Högberg, Structure and properties of phosphorus-carbide thin solid films, *Thin Solid Films* 548 (2013) 247-254.

[27] J.S. Kane and J.H. Reynolds, Mass spectrometer study of the vapors from red phosphorus and arsenic, *J. Chem. Phys.* 25 (1956) 342-349.

[28] S. Schmidt, C. Goyenola, G. K. Gueorguiev, J. Jensen, G. Greczynski, I. G. Ivanov, Zs. Czigány, and L. Hultman, Reactive high power impulse magnetron sputtering of CF_x thin films in mixed Ar/CF_4 and Ar/C_4F_8 discharges, .

[29] C. Goyenola, C.-C. Lai, L.-Å. Näslund, J. Lu, H. Högberg, L. Hultman, J. Rosen, and G. K. Gueorguiev, Theoretical prediction and synthesis of CS_xF_y thin films, *J. Phys. Chem. C* 120 (2016) 9527-9534.

[30] K. M. Eisele, SF6, a preferable etchant for plasma etching silicon, *J. Electrochem. Soc.* 128 (1981) 123-126.

[31] G. F. McLane and J. R. Flemish, High etch rates of SiC in magnetron enhanced SF_6 plasmas, *Appl. Phys. Lett.* 68 (1996) 3755-3757.

[32] C. C. Tang and D. W. Hess, Tungsten etching in CF_4 and SF_6 discharges, *J. Electrochem. Soc.* 131 (1984) 115-120.

[33] C. Goyenola, "Nanostructured carbon-based thin films: prediction and design" Thesis, Linköping University Electronic Press, 2015.

[34] M. J. Frisch et al., Gaussian 09, Gaussian Inc., Wallingford CT, (2009).

[35] J. P. Perdew, J. A. Chevary, S. H. Vosko, K. A. Jackson, M. R. Pederson, D. J. Singh, and C. Fiolhais, Atoms, molecules, solids, and surfaces: Applications of the generalized gradient approximation for exchange and correlation, *Phys. Rev. B* 46 (1992) 6671-6687.

[36] S. Stafström, L. Hultman, and N. Hellgren, Predicted stability of a new aza[60]fullerene molecule, $C_{48}N_{12}$, *Chem. Phys. Lett.* 340 (2001) 227-231.

[37] R.-H. Xie, G. W. Bryant, L. Jensen, J. Zhao, and V. H. Smith Jr., First-principles calculations of structural, electronic, vibrational, and magnetic properties of C_{60} and $C_{48}N_{12}$: A comparative study, *J. Chem. Phys.* 118 (2003) 8621-8635.

[38] W.C. Oliver and G.M. Pharr, An improved technique for determining hardness and elastic modulus using load and displacement sensing indentation experiments, *J. Mater. Res.* 7 (1992) 1564-1583.

[39] M. W. Chase Jr., Ed., NIST-JANAF Thermochemical Tables Fourth Edition Part I, Al-Co, American Institute of Physics, U.S.A., 1998.

[40] I. Sauers and G. Harman, A mass spectrometric study of positive and negative ion formation in an SF_6 corona. Part I: sources of sulphur-fluoride ions, *J. Phys. D: Appl. Phys.* 25 (1992) 761-773.

[41] A. Picard, G. Turban, and B. Grolleau, Plasma diagnostics of a SF_6 radiofrequency discharge used for the etching of silicon, *J. Phys. D: Appl. Phys.* 19 (1986) 991-1005.

[42] F. Y. Chu, SF_6 decomposition in gas-insulated equipment, *IEEE Trans. Electr. Insul.* EI-21 (1986) 693-724.

[43] R. d'Agostino and D. L. Flamm, Plasma etching of Si and SiO_2 in SF_6-O_2 mixtures, *J. Appl. Phys.* 52 (1981) 162-167.

[44] M. Kogoma and G. Turban, Mechanism of etching and of surface modification of polyimide in RF and LF SF_6-O_2 discharges, *Plasma Chem. Plasma Proc.* 6 (1986) 349-380.

[45] S. W. Youn, A. Ueno, M. Takahashi, and R. Maeda, A process of glassy carbon etching without the micro masking effect for the fabrication of a mold with a high-quality surface, *J. Micromech. Microeng.* 19 (2009) 125010.

[46] H. O. Pierson, 3 Graphite Structure and Properties in: Handbook of Carbon, Graphite, Diamond and Fullerenes, Noyes Publications, USA, 1993, pp. 43-69.

[47] S. Ravi, P. Silva, S. Xu, B. X. Tay, H. S. Tan, and W. I. Milne, Nanocrystalline in tetrahedral amorphous carbon films, *Appl. Phys. Lett.* 69 (1996) 491-493.

[48] S. Schmidt, G. Greczynski, C. Goyenola, G. K. Gueorguiev, Zs. Czigány, J. Jensen, I. G. Ivanov, and L. Hultman, CF_x thin solid films deposited by high power impulse magnetron sputtering: Synthesis and characterization, *Surf. Coat. Technol.* 206 (2011) 646-653.

[49] M. A. Tamor and W. C. Vassell, Raman "fingerprinting" of amorphous carbon films, *J. Appl. Phys.* 76 (1994) 3823-3830.

[50] A. Anders, A structure zone diagram including plasma-based deposition and ion etching, *Thin Solid Films* 518 (2010) 4087-4090.

[51] J. Neidhardt and L. Hultman, Beyond β - C_3N_4 —Fullerene-like carbon nitride: A promising coating material, *J. Vac. Sci. Technol. A* 25 (2007) 633-644.

[52] A. Bendavid, P. J. Martin, L. Randeniya, M. S. Amin, and R. Rohanizadeh, The properties of fluorine-containing diamond-like carbon films prepared by pulsed DC plasma-activated chemical vapour deposition, *Diam. Rlat. Mater.* 19 (2010) 1466-1471.

Supplementary Material to

Synthesis and properties of CS_xF_y thin films deposited by reactive magnetron sputtering in an Ar/SF_6 discharge

Chung-Chuan Lai*, Cecilia Goyenola, Esteban Broitman, Lars-Åke Näslund, Hans Högberg, Lars Hultman, Gueorgui K. Gueorguiev, and Johanna Rosen

Thin Film Physics Division, Department of Physics, Chemistry and Biology (IFM), Linköping University, SE-58183 Linköping, Sweden

* Corresponding author: Chung-Chuan Lai (chula@ifm.liu.se)

XPS spectra of C 1s, S 2p, and F 1s regions from the CS_xF_y thin film samples

Fig. S1 shows XPS spectra acquired around C 1s region of the CS_xF_y thin films deposited with P_{SF6} = 1.0 mPa, 1.5 mPa, and 2.0 mPa (from top to bottom of the figure). The most prominent features are marked with numbers (1) – (5) respectively from low to high binding energy (BE). The two samples grown at the same condition, i.e. with P_{SF6} = 2.0 mPa, have very similar features in the C 1s spectra with each other, in consistence with other analysis techniques. The feature (1) at BE ~ 284.5 – 284.7 eV can be identified as the most characteristic C – C sp^2 component, which is shifting towards higher BE when increasing P_{SF6}. This can be related to the increment of overall F content in the material and consequently the C – C sp^2 component is more affected by surrounding C – F bonds. The position of the feature (1) in the samples grown at P_{SF6} = 2.0 mPa is close to the position reported by Schmidt et al. in the CF_x samples with high F content (> 15.5 at.%) [1]. In addition, the low degree of asymmetry for (1) indicates a low contribution from feature (2), which can be assigned to C – C sp^3 component at BE ~ 285.9 eV, as compared to Ref. [1]. It is reasonable that in the growth condition lacking of energetic ion bombardment, e.g. in DCMS, the content of C – C sp^3 bond is low in the samples, as compared to growth condition utilizing high substrate bias or HiPIMS. The features (3) – (5) can be assigned to the components of C – F/C – CF_2 at ~ 287.2 eV, C – F_2/ C – CF_3 at ~ 290.0 eV, and C – F_3 at ~ 292.2 eV, respectively, and line up well with the same components reported in Ref. [1]. The increase in (3) – (5) and the decrease in (1) indicate that, upon increasing P_{SF6}, more F atoms are bonded to C atoms in the network, inhibiting the formation of C – C sp^2 bond.

Due to similar electronegativity for C and S atoms, the C 1s feature is less affected by introducing S atoms into the C network. It has been reported by Chang that the C – C sp^2 component is located at BE ~ 284.3 – 284.5 eV in

C-S compound samples with S > 24 wt.% (~ 16 at.%) [2]. In our case, the S content is less than 1.5 at.% in all samples, and hence the effect of S atoms on C 1s components is possibly not distinguishable.

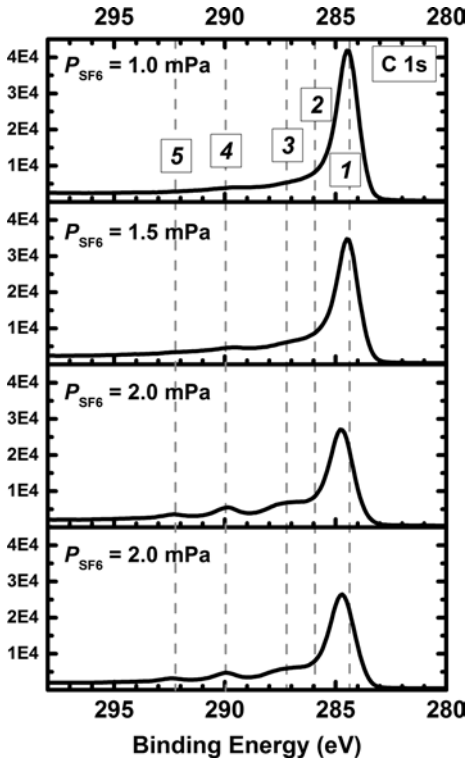

Figure S1. XPS spectra of the CS_xF_y samples acquired at C 1s regions. The main features are marked with numbers (1) – (5) and respective dashed lines.

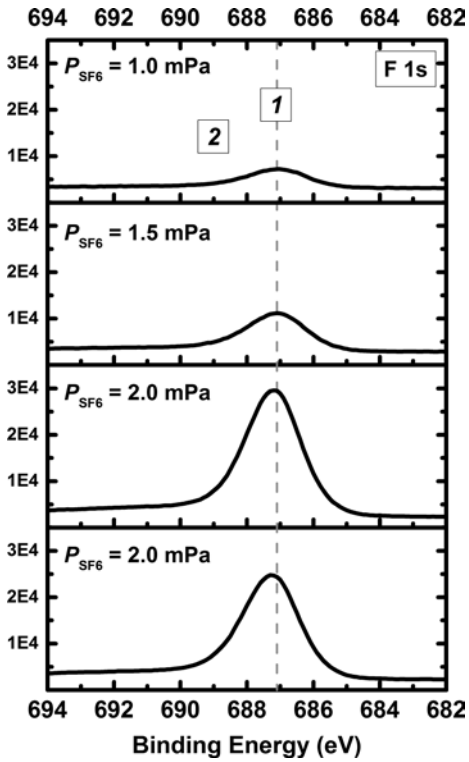

Figure S2. XPS spectra of the CS_xF_y samples acquired at F 1s regions. The main features are marked with numbers (1) – (2) and respective dashed lines.

Fig. S2 shows XPS spectra acquired around F 1s region of the CS_xF_y samples deposited with P_{SF6} = 1.0 mPa, 1.5 mPa, and 2.0 mPa (from top to bottom of the figure), where the most prominent features are again marked with numbers (1) – (2) respectively from low to high BE. The main F 1s feature, marked as (1), is located at BE ~ 687.0 – 687.2 eV, shifting towards higher BE and increasing in intensity along with increasing P_{SF6}. The position of (1) is similar to published values for covalent C – F bonds as in the organic compounds, while no sign of more ionic F bond with BE < 685 eV is observed [3]. Similar to the case in C 1s, the shift of (1) towards higher BE is related to the effect of higher F content in the material, and therefore a higher number of adjacent C – F bonds. The feature at higher BE side, marked as (2), is assigned to the components of perfluorinated groups or alternatively plasmon effects from (1) [3].

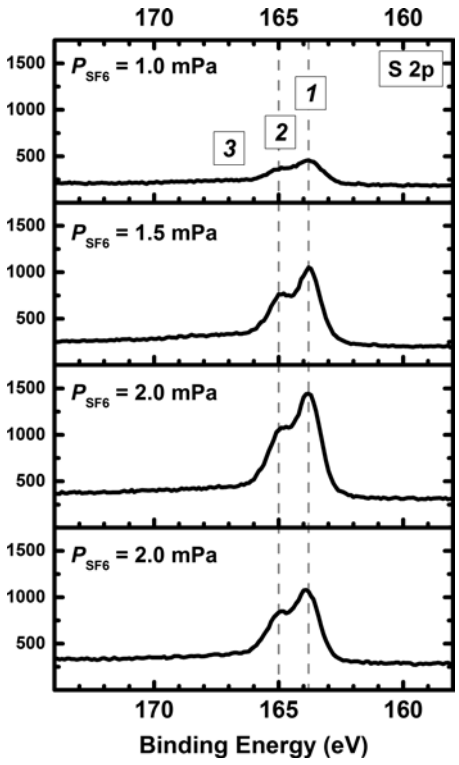

Figure S3. XPS spectra of the CS_xF_y samples acquired at S 2p regions. The main features are marked with numbers (1) – (3) and respective dashed lines.

Fig. S3 shows XPS spectra acquired around S 2p region of the CS_xF_y samples deposited with P_{SF6} = 1.0 mPa, 1.5 mPa, and 2.0 mPa (from top to bottom of the figure), where the most prominent features are again marked with numbers (1) – (3) respectively from low to high BE. Features (1) and (2) can be assigned to S $2p_{3/2}$ at BE ~ 163.8 eV and S $2p_{1/2}$ at BE ~ 165.0 eV, respectively for S bonded in C-S compounds [2]. No indication in the S 2p region shows other form of S in the samples, such as metal sulfides (160 – 163 eV), sulfates (168 – 170 eV), or elemental sulfur (~163.1 eV) [2] [4].

References

[1] S. Schmidt, C. Goyenola, G. K. Gueorguiev, J. Jensen, G. Greczynski, I. G. Ivanov, Zs. Czigány, and L. Hultman, Reactive high power impulse magnetron sputtering of CF_x thin films in mixed Ar/CF_4 and Ar/C_4F_8 discharges, *Thin Solid Films* 542 (2013) 21-30.

[2] C. H. Chang, Preparation and characterization of carbon-sulfur surface compounds, *Carbon* 19 (1981) 175-186.

[3] A. Tressaud, F. Moguet, S. Flandrois, M. Chambon, C. Guimon, G. Nanse, E. Papirer, V. Gupta, and O. P. Bahl, On the nature of C-F bonds in various fluorinated carbon materials: XPS and TEM investigations, *J. Phys. Chem. Solids* 57 (1996) 745-751.

[4] D. Lichtman, J. H. Craig Jr., V. Sailer, and M. Drinkwine, AES and XPS spectra of sulfur in sulfur compounds, *Appl. Surf. Sci.* 7 (1981) 325-331.